Article

The Lantibiotic Nisin Induces Lipid II Aggregation, Causing Membrane Instability and Vesicle Budding

Katharina M. Scherer,[1,*] Jan-Hendrik Spille,[1] Hans-Georg Sahl,[2] Fabian Grein,[2] and Ulrich Kubitscheck[1]

[1]Institute for Physical and Theoretical Chemistry and [2]Institute for Medical Microbiology, Immunology and Parasitology, Pharmaceutical Microbiology Unit, Rheinische Friedrich-Wilhelms University Bonn, Bonn, Germany

ABSTRACT   The antimicrobial peptide nisin exerts its activity by a unique dual mechanism. It permeates the cell membranes of Gram-positive bacteria by binding to the cell wall precursor Lipid II and inhibits cell wall synthesis. Binding of nisin to Lipid II induces the formation of large nisin-Lipid II aggregates in the membrane of bacteria as well as in Lipid II-doped model membranes. Mechanistic details of the aggregation process and its impact on membrane permeation are still unresolved. In our experiments, we found that fluorescently labeled nisin bound very inhomogeneously to bacterial membranes as a consequence of the strong aggregation due to Lipid II binding. A correlation between cell membrane damage and nisin aggregation was observed in vivo. To further investigate the aggregation process of Lipid II and nisin, we assessed its dynamics by single-molecule microscopy of fluorescently labeled Lipid II molecules in giant unilamellar vesicles using light-sheet illumination. We observed a continuous reduction of Lipid II mobility due to a steady growth of nisin-Lipid II aggregates as a function of time and nisin concentration. From the measured diffusion constants of Lipid II, we estimated that the largest aggregates contained tens of thousands of Lipid II molecules. Furthermore, we observed that the formation of large nisin-Lipid II aggregates induced vesicle budding in giant unilamellar vesicles. Thus, we propose a membrane permeation mechanism that is dependent on the continuous growth of nisin-Lipid II aggregation and probably involves curvature effects on the membrane.

INTRODUCTION

Antimicrobial peptides (AMPs) exhibit activity against bacteria, viruses, and fungi. They are structurally as diverse as their mechanisms of action. However, particularly short (<40 amino acids) cationic AMPs have a common feature: they are disordered in aqueous solution but adopt an amphipathic structure in the presence of micelles and membranes (1). This enables them to attack bacteria by inserting into the bacterial cell membrane. Self-assembly of the peptides on the bacterial cell membrane can lead to pore formation or membrane disruption. Different membrane-perforation mechanisms exist depending on the orientation of the peptides to the membrane plane. The aggregation of peptides oriented parallel to the membrane plane may lead to a detergent-like solubilization of the membrane (2), whereas peptides, which undergo a transition from a parallel to a perpendicular orientation, are able to form membrane-spanning oligomers such as barrel-stave (3) or toroidal pores (4). Recent molecular-dynamics simulations suggested that these pores are not as stable and ordered as previously assumed (5).

Further mechanisms by which AMPs kill target cells include the inhibition of vital biological functions such as cell wall biosynthesis and the synthesis of DNA, RNA, and specific proteins (1). The positively charged lantibiotic nisin displays a unique killing mechanism on Gram-positive bacteria by binding to a specific cell membrane target. This target, Lipid II, is a component of the cell wall biosynthesis machinery. It is composed of the membrane anchor undecaprenyl-pyrophosphate, two phosphate groups, and a peptidoglycan subunit.

Nisin belongs to the pore-forming class I bacteriocins, and its membrane-permeating capability was shown to be increased by two orders of magnitude when Lipid II was present in the membrane (6). Based on structural studies of the nisin-Lipid II complex, investigators proposed the following pore-formation mechanism: First, nisin would bind to Lipid II with the two lanthionine rings of its N-terminus, thus forming a pyrophosphate cage around the headgroup of Lipid II (7). The flexible hinge region in the center of the nisin molecule would then allow insertion of its C-terminus into the membrane, probably accompanied by a change from a parallel to a transmembrane orientation of the peptide (8). Accumulation of these complexes in the membrane would finally lead to stable pores, as suggested by black lipid membrane studies (9). The stoichiometry of nisin and Lipid II required for maximal pore formation was determined to be 2:1 (10).

Yet, in the bacterial cell, binding of nisin to Lipid II not only leads to pore formation but also inhibits cell wall biosynthesis due to interruption of the multienzymatic peptidoglycan production cycle (6). This inhibition is caused by the segregation of Lipid II by nisin. Large

http://dx.doi.org/10.1016/j.bpj.2015.01.020

CrossMark

aggregates of fluorescently labeled nisin were observed on Lipid II-containing membranes of giant unilamellar vesicles (GUVs) as well as on the bacterial cell membrane (11). In vitro analysis showed that the efficiency of nisin membrane permeation correlated with aggregate size (12). The brightness of aggregates of fluorescently labeled nisin in vitro as well as in vivo indicates a high number of accumulated nisin molecules and therefore a strong aggregation tendency of nisin and Lipid II. This raises a question about the functional relevance of stable pores of a finite and relatively small size, comprising only a few molecules (13).

Therefore, we first analyzed the possible biological relevance of large aggregates with regard to the killing effect of nisin. Cells of *Bacillus subtilis* were incubated with fluorescently labeled nisin. Nisin bound inhomogeneously to the bacterial membranes and induced the formation of aggregates of different sizes. Cell death directly correlated with the existence of large aggregates in the membrane. To gain further insight into the aggregation and perforation process, we then studied the dynamics of Lipid II aggregation and estimated the aggregate size by a quantitative analysis. To this end, we examined the motion of single, fluorescently labeled Lipid II molecules in GUVs upon addition of nisin by means of light-sheet fluorescence microscopy (LSFM) (14). We observed that the mobility of Lipid II molecules was reduced continuously due to an increasing size of the Lipid II-nisin aggregates. The reduction in mobility was dependent on the interaction time and nisin concentration. From the measured diffusion coefficients, we were able to estimate the corresponding aggregate sizes. Furthermore, the nisin-induced aggregation of Lipid II also led to GUV destruction and shrinking due to vesicle budding. Thus, we propose that the killing mechanism of nisin involves severe structural membrane deformations due to Lipid II-nisin aggregation.

MATERIALS AND METHODS

Chemicals and compounds

All chemicals used in this work were of analytical grade or better. Low melting point agarose (AppliChem, Darmstadt, Germany) was used to prepare agarose pads for immobilization of bacteria. SYTOX Green nucleic acid stain (Invitrogen, Karlsruhe, Germany) was used for cell viability staining of bacteria. The phospholipids 1-palmitoyl-2-oleoyl-*sn*-glycero-3-phosphocholine (POPC) and 1-palmitoyl-2-oleoyl-*sn*-glycero-3-phosphoethanolamine (POPE) were purchased from Avanti Polar Lipids (Alabaster, AL) and used without further purification. Lipids were dissolved in chloroform to a final concentration of 1.3 mM. Undecaprenyl-diphosphate (C_{55}-PP) was purchased from Larodan (Malmo, Sweden) and used for Lipid II synthesis. Alexa Fluor 546-NHS-ester (AF546; Invitrogen) and Atto647-NHS-ester (Atto647; Sigma Aldrich, Schnelldorf, Germany) were used for lipid labeling. Nisin was labeled with Alexa Fluor 647-hydrazide (AF647; Invitrogen). The hydrophilic dye Lucifer Yellow (LY) was purchased from Invitrogen.

At least four natural variants of nisin are known (15–18). In our studies, we used nisin Z and simply refer to it as nisin and, for the fluorescently labeled molecule, nisin-AF647. Nisin was purified from culture superna-

tants of *Lactococcus lactis* NIZO22186 (19) by chloroform extraction and high-performance liquid chromatography (20). Purified nisin was lyophilized and stored at −20°C. Stock solutions were prepared in 0.005% acetic acid. The carboxyl group of nisin was labeled with AF647 and the compound was purified according to Scherer et al. (12). The lipid-bound cell wall precursor Lipid II was synthesized in vitro and purified as described previously (21). All reaction products were extracted by butanol/6M pyridine acetate, pH 4.2, and analyzed by thin-layer chromatography (TLC). Lipids were fluorescently labeled by coupling AF546-NHS-ester or Atto647-NHS-ester to the amino group of the phospholipid POPE, and Atto647-NHS-ester to the amino group of the lysine residue of Lipid II. For POPE labeling, the reaction was carried out with 30 nmol POPE and an equimolar amount of dye in chloroform/methanol (2:1, v/v) for 1 h at room temperature upon addition of 15 molar equivalents of triethylamine (NEt_3) according to Moumtzi et al. (22). Separation of labeled and nonlabeled lipids was achieved by preparative TLC using chloroform/methanol/water (65:25:4, v/v/v) as solvent. Then, 5 nmol Lipid II was labeled with 2.5 molar equivalents of dye in chloroform/methanol/*N,N*-diisopropylethylamine (5:5:1, v/v/v). The assay was briefly mixed and incubated for 1 h at room temperature with gentle agitation. Separation of labeled and nonlabeled lipids was achieved by preparative TLC using chloroform/methanol/water/ammonia (88:48:10:1, v/v/v/v) as solvent. The bands corresponding to the labeled lipids were scratched from the TLC plates and the desired products were extracted from the silica using methanol.

Fluorescence microscopy of bacteria

A culture of *B. subtilis* 168 was grown in lysogeny broth (LB) medium at 37°C to an OD_{600} of 0.25. Cells were centrifuged, washed with M9 medium, and resuspended in 1/10 of the starting volume. Then, 10 μL of concentrated cells in M9 medium were incubated for 5 min with 1.5 μM nisin-AF647, and 1 μl of the treated cells was applied on an agarose pad (1% low melting point agarose in M9 medium, 50 nM SYTOX Green). The inverted agarose pad was then placed in a microscopy chamber (MatTek, Ashland, MA) and imaged with an inverted microscope using an 100× objective lens with an NA 1.46 (Zeiss, Jena, Germany) and a 4× magnifier onto an EMCCD camera (iXon DU-897D; Andor Technology, Belfast, Northern Ireland); 2 × 2 binning during acquisition resulted in a pixel size of 80 nm. Images were taken 15–25 min after immobilization. Images were recorded using transmitted light as well as laser excitation at 488 nm (Sapphire-100; Coherent, Santa Clara, CA) for SYTOX Green and 640 nm (Cube640-40C; Coherent) for nisin-AF647. Fluorescence was filtered using the appropriate notch filters (NF03-488E-25 and NF01-633-U-23.7-D; both Semrock, Lake Forest, IL). To analyze the correlation between cell damage and nisin aggregation, we calculated the maximum intensities of SYTOX Green and nisin-AF647 for 80 cells by determining the maximum pixel intensity of single cells.

GUV and sample preparation

GUVs were prepared by electroformation (23,24) in 250 mM sucrose solution as described previously (25). Vesicles consisted of POPC or a mixture of POPC and 0.2 mol % Lipid II. Labeled probes were added to observe the GUV membrane (10^{-3} mol % POPE-AF546 or POPE-Atto647) and for single-particle tracking (10^{-6} mol % POPE-Atto647 or Lipid II-Atto647). For measurements, 250 mM glucose solution in deionized water was mixed with nisin or nisin-AF647 before GUV addition, and GUVs were diluted 1:8.25 in this mixture. For translocation experiments, 20 μM of the tracer dye LY was mixed with the nisin-sugar solution before addition of GUVs. In the microscopy chamber, GUVs sedimented due to the density difference between the sucrose and glucose solutions. Data acquisition was started after a 5 min incubation period, during which time the vesicles resided in a stable position at the chamber bottom.

GUV imaging

GUVs were transferred to a custom-made sample chamber (26) and imaged by LSFM. Fluorescence was excited by illumination with either one of three laser lines (488 nm (Sapphire-100; Coherent), 640 nm (Cube640-40C; Coherent), and 532 nm (LasNova GLK 3250 T01; LASOS Lasertechnik, Jena, Germany)) in a thin sheet (2.2 μm full width at half-maximum (FWHM)) orthogonal to the detection axis. For tracking experiments, the upper surface of the GUVs was observed. Fluorescence was collected by a high numerical aperture objective lens (CFI Apo LWD Lambda S 40× NA 1.15; Nikon, Tokyo, Japan), filtered using the appropriate notch (NF01-633-U-23.7-D; Semrock) and band-pass (z532/640m; Chroma, Bellows Falls, VT) filters, and detected with an EMCCD camera (iXon DV-860; Andor Technology). An additional 2.5× magnification lens led to a pixel size of 240 nm. Movies with 2000 images at a frame rate of 95 Hz were recorded in frame transfer mode.

For translocation measurements, fluorescence was imaged at lower magnification (Plan Fluor 20× NA 0.5; Nikon) through an appropriate notch filter (NF01-488-U-23.7-D; Semrock) onto a pco.edge sCMOS camera (pco.edge; PCO, Kelheim, Germany). An image was taken every 30 s over a period of 20 min. Membrane perforation of nisin was quantitatively analyzed by the translocation of LY across GUV membranes. The fluorescence intensities inside, F_{in}, and outside, F_{out}, of GUVs with a radius larger than 20 μm were determined at 7.5, 12.5, 17.5, and 22.5 min after addition of nisin using ImageJ (27). The ratio F_{in}/F_{out} was used as a measure for membrane permeation.

Volumetric imaging was performed at lower magnification (CFI Plan Fluor 10× NA 0.30; Nikon) and with a light sheet of 10 μm thickness (FWHM) using the pco.edge camera. One image stack per minute was obtained by moving the sample through the light sheet and acquiring an image every 1 μm. The total acquisition time per stack was 4 s. For simultaneous detection of two colors, a dual emission image splitter (OptoSplit II; Cairn Research Ltd, Faversham, UK) was inserted in front of the pco.edge camera. A dichroic mirror (FF662-FDi01-25x36; Semrock) and a band-pass emission filter (ET560/80M, Chroma) were used to separate the emission channels. Image separation was adjusted so that the camera chip was fully illuminated and the two spectrally resolved images covered equal areas. To measure the vesicle radius as a function of time, radii of GUVs were determined manually from sum projections of individual stacks.

Single-particle tracking and analysis

Particles were tracked using Diatrack (Semasopht, Chavannes, Switzerland). Curve fitting was performed with Origin (OriginLab, Northampton, MA). All further data evaluation was performed using either Origin or MATLAB (The MathWorks, Natick, MA).

First, trajectories were grouped into time intervals. For each time interval, a mean-square displacement (MSD) curve was determined and fitted as previously described (28). For all trajectories with more than two jumps, square displacements $r^2(n\Delta t)$ (Δt = inverse frame rate) were calculated for all differences of the running index $n = 1, ..., N - 1$. The MSDs $<r^2(n\Delta t)>$ were determined by averaging all available square displacements of identical values $n\Delta t$ and plotted against time. Diffusion coefficients D were finally obtained by fitting the data to $<r^2(n\Delta t)> = 4Dn\Delta t$ (28).

Diffusion coefficients were also calculated from histograms of the jump distances (JDs) r according to

$$P(r, \Delta t) = \sum_{i=1}^{m} \frac{A_i}{2D_i} \times e^{-\frac{r^2}{4D_i\Delta t_c}} \cdot r \qquad (1)$$

with A_i ($\sum_{i=1}^{m} A_i = 1$) (29) designating the relative fractions of the diffusion coefficients D_i that corresponded to different diffusive species or states.

Similarly, the cumulative distribution of the square displacements r^2 (28) could be fitted with the following function:

$$P'(r, \Delta t) = 1 - \sum_{i=1}^{m} A_i \cdot e^{-\frac{r^2}{4D_i\Delta t_c}}. \qquad (2)$$

Equation 2 avoided a possible loss of information and bias introduced by histogram binning. We calculated $P'(r, \Delta t)$ by counting the number of values $\leq r^2$ and normalizing to the total number of data points (29). For both evaluation methods, only trajectories with more than two jumps were considered.

To determine the distribution of diffusion coefficients D, we determined D from an MSD analysis of single trajectories by linear curve fitting of the first three data points. The shortest trajectories sometimes yielded negative or very large D values. The fit results of these short trajectories were characterized by low values for the goodness of fit assessed by the normalized χ^2 value. Thus, only results with $\chi^2 > 0.9$ were taken into account. The goodness of fit χ^2 was determined as $\chi^2 = 1 - SSE/SST$ (where SSE is the summed square of residuals and SST is the total sum of squares) and could take values of zero to one.

Determination of aggregate size

For the calculation of lipid radii from the diffusion coefficients D, we used the classical expression derived by Saffman and Delbrück (30):

$$D = \frac{k_B T}{4\pi\mu_m h} \cdot \ln\left(\frac{\mu_m h}{\mu_w R} - \gamma\right) \qquad (3)$$

where T is the temperature, h is the membrane thickness, μ_m is the membrane viscosity, μ_w is the viscosity of the surrounding medium, R is the particle radius, and Euler's constant $\gamma = 0.577215$.

However, this widely used model is only valid for small objects embedded in a membrane. A more general model was developed by Hughes et al. (31). This model is also valid for larger objects, but requires a numerical computation of D. An analytical approximation was proposed by Petrov and Schwille (32):

$$D = \frac{k_B T}{4\pi\mu_m h} \cdot \frac{\left[\ln\left(\frac{2}{\varepsilon}\right) - \gamma + \frac{4\varepsilon}{\pi} - \left(\frac{\varepsilon^2}{2}\right)\ln\left(\frac{2}{\varepsilon}\right)\right]}{\left[1 - \frac{\varepsilon^3}{\pi}\ln\left(\frac{2}{\varepsilon}\right) + \frac{c_1\varepsilon^{b_1}}{1 + c_2\varepsilon^{b_2}}\right]} \qquad (4)$$

with the reduced radius $\varepsilon = (R\mu_w/\mu_m h)$, $c_1 = 0.73761$, $b_1 = 2.74819$, $c_2 = 0.52119$, and $b_2 = 0.61465$. We used this expression to estimate the radii of Lipid II-nisin aggregates by numerically solving for R.

RESULTS

Several previous studies investigated the pore-formation mechanism of small nisin oligomers as a putative cause of cell death (6,9,13). Hasper et al. (11) discovered the formation of large nisin aggregates both in vitro and in vivo, and suggested an alternative killing mechanism by which nisin inhibits cell wall biosynthesis in bacterial cells by segregating Lipid II.

Aggregate formation in vivo

To examine the biological relevance of large nisin-Lipid II aggregates, we incubated cells of *B. subtilis* with 1.5 μM of nisin-AF647. Membrane integrity and cell viability were examined with the use of SYTOX Green. Due to its

three positive charges, this dye is not membrane permeant; rather, it only penetrates damaged membranes and then specifically stains nucleic acids. Thus, it can be used as marker for membrane disruption and dead cells (33).

Fig. 1 A shows example images of immobilized cells incubated with nisin-AF647. Generally, the distribution of the peptide in the cell membrane was not homogeneous, and instead aggregates with different intensities and dimensions were visible. Cells exhibiting aggregates of low fluorescence intensity did not show any damage as judged by a missing SYTOX Green signal. Only bright and thus large aggregates caused membrane disruption and cell death as indicated by increased SYTOX Green fluorescence. Large aggregates were mostly detected in the centers of cells (where the septum is formed) and at cell poles, both regions of Lipid II synthesis and activity. The visual impression was corroborated by a quantitative analysis of the maximum intensity of SYTOX Green and nisin-AF647 in 80 bacterial cells
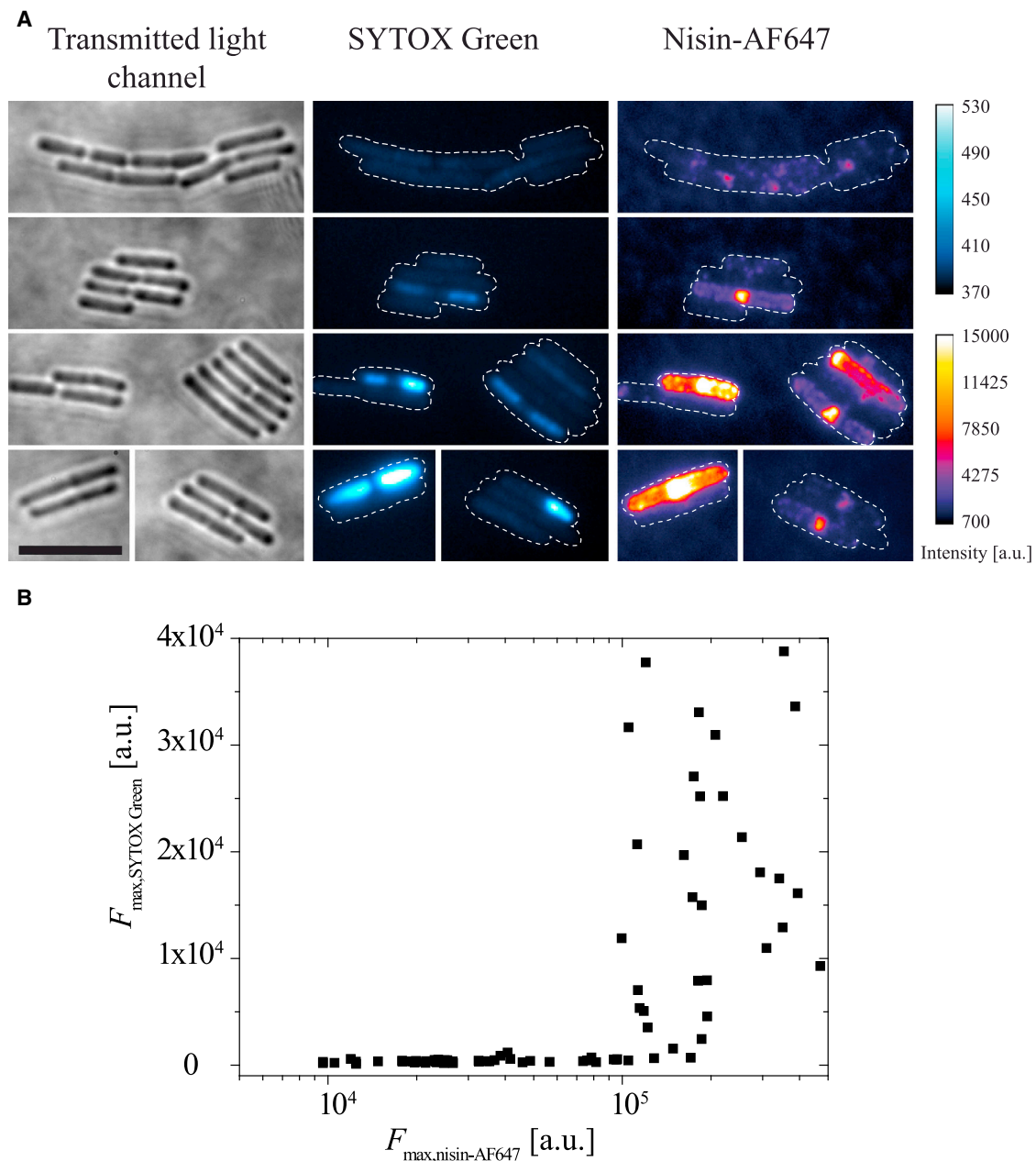

FIGURE 1 Membrane rupture and cell death correlated with the occurrence of nisin-Lipid II clusters. (A) *Bacillus subtilis* cells treated with 1.5 μM nisin-AF647. Cells were incubated with fluorescent nisin for 5 min and then immobilized on agarose pads containing 50 nM SYTOX Green. Images were taken 15–25 min after immobilization. Left: transmitted light images of the bacteria; center: SYTOX Green fluorescence; right: nisin-AF647 fluorescence. Clusters of *B. subtilis* cells are outlined with a dashed white line. Scale bar, 10 μm. Corresponding lookup tables of the fluorescence intensities are shown. (B) Plot of maximum SYTOX Green fluorescence as a function of maximum nisin-AF647 fluorescence within single cells ($N = 80$). To see this figure in color, go online.

(Fig. 1 B). The plot demonstrated that an increase in SYTOX Green fluorescence was only observed for cells that exhibited a nisin-AF647 intensity beyond a certain threshold. We did not observe an increased SYTOX Green fluorescence without the presence of discernible nisin aggregates. This suggested that a minimum aggregate size was required to efficiently disrupt the membranes and kill the cells.

Mobility of lipid tracers and single Lipid II molecules

To investigate the aggregation process of nisin under well-controlled conditions, we used GUVs as a membrane model system. First, we characterized the model system by measuring the membrane viscosity and effective radius of Lipid II. Membrane viscosity and particle size determine molecular mobility in membranes. Therefore, we determined the mobility of fluorescently labeled POPE and Lipid II molecules in GUV membranes formed by POPC (Fig. 2 A). Light-sheet illumination provided intrinsic optical sectioning and enabled single-molecule observation with an exceptionally high signal/noise ratio (SNR) (26).

We measured the diffusion coefficients of Lipid II-Atto647 and POPE-Atto647 by single-molecule tracking in the upper bilayer of the GUVs (Fig. 2 B; Movie S1 in the Supporting Material). We performed these measurements using a very high dilution of labeled lipids in the
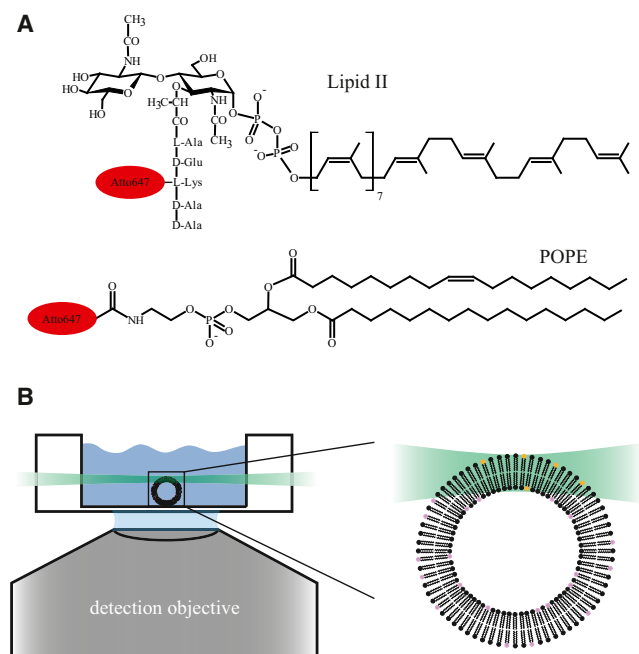

FIGURE 2   Imaging of single lipid tracer molecules. (A) Molecular structures of the lipid tracers POPE and Lipid II labeled with Atto647. (B) Scheme of light-sheet illumination of the GUVs. GUVs were imaged in a custom-built glass cuvette. The sectioning effect of the light sheet was used to excite fluorescence only in the upper surface of the GUVs. To see this figure in color, go online.

membrane (10^{-6} mol %), which allowed us to observe and track spatially well-separated single-molecule signals. We evaluated diffusion coefficients D_{MSD} from the time-dependent MSD, D_{CD} from the cumulative distributions of square displacements, and D_{JD} from the JD histograms. The data are shown in Fig. S1 A. The diffusion coefficients thus determined are summarized in Table S1. To determine the membrane viscosity, we used POPE-Atto647 as a tracer molecule. We supposed that diffusion of POPE-Atto647 was determined only by the lipid tails in the membrane, which were the same as observed for POPC. For POPE-Atto647, we obtained diffusion coefficients with slightly higher values than those obtained for Lipid II-Atto647, probably due to a smaller effective molecular radius of the phospholipids compared with Lipid II (Table S1; Fig. S1 B).

Applying literature values for the membrane thickness ($h = 3.98$ nm) and lipid area ($a = 0.63$ nm^2, $R_{POPC} = 0.45$ nm for a circular area) of POPC bilayers (34), the viscosity of 250 mM sugar solutions ($\mu_w = (1.16 \pm 0.14) \times 10^{-3}$ Pa·s at 20°C) (35), and a diffusion coefficient $D_{CD} = 5.1 \pm 0.03$ μm^2/s for POPE-Atto647, we calculated a POPC membrane viscosity of $\mu_{m,POPC} = 0.106$ Pa·s using Eq. 3. Correspondingly, the effective radius of Lipid II-Atto647 was determined as $R_{LII} = 0.59 \pm 0.23$ nm.

In later experiments, we used a higher Lipid II concentration in the membrane to study aggregation upon addition of nisin. To approximate the Lipid II concentration in bacterial membranes where the maximal ratio of Lipid II/phospholipids was determined as 1:100 (36), we incorporated 0.2 mol % nonfluorescent Lipid II into POPC GUVs in addition to the 10^{-6} mol % Lipid II-Atto647. This yielded a Lipid II/phospholipid ratio of 1:500, whereas only one out of 200,000 Lipid II molecules carried a fluorescent label. We speculated that this (higher) Lipid II concentration might alter the overall membrane viscosity. To test for this and for possible interactions among the Lipid II molecules, we again measured the mobility of POPE-Atto647 and Lipid II-Atto647 in these bilayers (Fig. S1, C and D). The obtained diffusion coefficients reflected a slightly increased mobility of both molecules compared with pure POPC bilayers (Table S1). We calculated the membrane viscosity of the GUVs containing 0.2 mol % Lipid II using the same literature values as before, under the assumption of unaltered lipid area and membrane thickness, and obtained a reduced value of $\mu_{m,LII} = 0.097$ Pa·s. Since the increase in the value of the diffusion coefficients was observed for both Lipid II-Atto647 and POPE-Atto647, a specific interaction between individual Lipid II molecules was excluded.

We attribute the slight decrease in membrane viscosity to the relatively high number of Lipid II molecules. Their long, highly flexible bactoprenol tail is known to increase the disorder in bilayer organization (37), which probably increases the membrane fluidity. Again, Lipid II-Atto647 exhibited a lower diffusion coefficient than POPE-Atto647.

For all further measurements, membranes with 0.2 mol % Lipid II were prepared.

Nisin-induced mobility reduction of Lipid II

Next, we examined Lipid II mobility after addition of nisin to Lipid II-containing GUV membranes as a function of time. Two different concentrations of nisin, 0.2 μM and 1.5 μM, were added to the vesicles, resulting in nisin/Lipid II ratios of 4:1 and 30:1, respectively. The minimum inhibitory concentration (MIC) of nisin Z is in the range of 5–300 nM depending on the tested bacterial strains (38). Thus, the concentration of 0.2 μM nisin resides well in that range, whereas 1.5 μM nisin provides a concentration at least 5-fold higher than the MIC. An excess of nisin over Lipid II was chosen in both cases to ensure that aggregate formation would be detectable.

For each concentration, six different samples were prepared, and in each sample the mobility of Lipid II-Atto647 was measured on three to five different GUVs. Measurements began 5 min after addition of nisin and continued for 20 min. Trajectories were binned in 5 min time intervals to yield sufficient statistical information for the analysis. We evaluated the trajectories using different approaches because each method revealed a different aspect of the physical processes reflected by the changes in Lipid II mobility.

First, mean diffusion coefficients were evaluated for each time interval from the respective MSD curve (Fig. 3). For both nisin concentrations, a time-dependent decrease of Lipid II mobility was found. The mobility reduction was most likely due to the increasing size of the molecular aggregates formed by nisin and Lipid II. The effect was more pronounced for the higher nisin concentration. The values of the diffusion coefficients D_{MSD} are summarized in Table 1.

MSD curves provide only mean diffusion coefficients. A more detailed picture can be obtained from the distributions

TABLE 1 Diffusion constants of Lipid II-Atto647 from MSD evaluation

Time interval	D_{MSD} [μm^2/s] for 0.2 μM nisin	D_{MSD} [μm^2/s] for 1.5 μM nisin
5–10 min	5.3 ± 0.1	4.6 ± 0.1
10–15 min	5.1 ± 0.1	4.8 ± 0.1
15–20 min	4.7 ± 0.1	4.7 ± 0.1
20–25 min	4.6 ± 0.1	4.3 ± 0.1

Time-dependent mobility of Lipid II-Atto647 in 0.2 mol % Lipid II-containing POPC GUVs upon addition of nisin.

of the diffusion coefficients because they also reflect the size distribution of the diffusing species. Thus, we calculated the diffusion coefficients of single Lipid II trajectories as described in Materials and Methods. The results were plotted as cumulative distribution functions (Fig. S2).

Since single-molecule trajectories are of a stochastic nature, the diffusion coefficients varied largely even without addition of nisin. However, changes upon nisin addition compared with this zero level were clearly observed. As expected, the distributions showed a continuous shift toward lower diffusion coefficients with increasing incubation time. Again, this effect was more pronounced for the higher nisin/Lipid II ratio. The addition of nisin led to an increase in the number of trajectories with lower diffusion coefficients, indicating a continuous growth in the number of aggregates in time.

Lipid II-nisin aggregates contain thousands of molecules

We then analyzed the JD distributions of the trajectories that accumulated during the different time intervals to identify different fractions of mobile species. Fig. S3 presents the cumulative distributions of the squared JDs fitted by Eq. 2. To minimize parameter correlations between the fitting parameters A_i and D_i, we reduced the number of free parameters by sharing the diffusion constants D_i among all eight distributions in a global fit (39). Three mobility fractions were required to satisfactorily describe the combined data set with diffusion constants $D_1 = 5.1 \pm 0.02$ μm^2/s, $D_2 = 2.6 \pm 0.05$ μm^2/s, and $D_3 = 0.3 \pm 0.02$ μm^2/s.

Fig. 4 A shows example trajectories representing the diffusion coefficients D_1, D_2, and D_3. JD distributions provide a way to depict these diffusion coefficients D_i and their relative fractions A_i. Fig. 4 B shows the distribution corresponding to single Lipid II molecules, which could well be represented by the diffusion coefficient D_1 alone. Therefore, we attributed D_1 to the diffusion of single Lipid II-Atto647 molecules. The diffusion coefficients D_2 and D_3 were ascribed to intermediate and large nisin-Lipid II aggregates, respectively.

Differences in Lipid II-AF647 diffusion after addition of nisin were visible in the JD distributions (Fig. 4, C and D; see Fig. S4 for additional time intervals). The relative
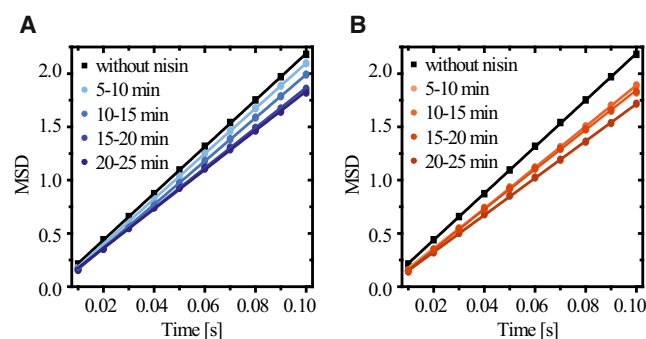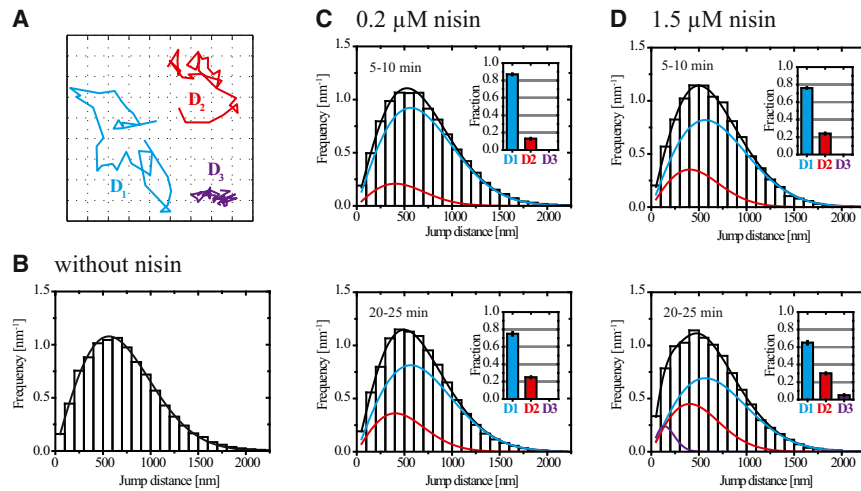

FIGURE 3 MSD curves for Lipid II-Atto647 mobility. (A and B) MSD curves quantifying Lipid II-Atto647 diffusion in POPC membranes after addition of (A) 0.2 μM nisin and (B) 1.5 μM nisin. MSDs were calculated for 5 min intervals over an overall observation time of 20 min. Time intervals are given in the figure. With increasing observation time, the slope of the MSD decreased. Black curves show the MSD curve of single Lipid II molecules without addition of nisin. To see this figure in color, go online.

A

C 0.2 µM nisin

D 1.5 µM nisin

B without nisin

FIGURE 4 JD histograms for Lipid II-Atto647 mobility. (*A*) Example trajectories representing the diffusion coefficients $D_1 = 5.1$ μm^2/s, $D_2 = 2.6$ μm^2/s, and $D_3 = 0.3$ μm^2/s. (*B–D*) JD histograms for Lipid II-Atto647 trajectories without addition of nisin (*B*) and upon addition of 0.2 μM (*C*) and 1.5 μM (*D*) nisin. For each nisin concentration, two time intervals are shown. Black curves show the fit for the whole distribution, and blue, red, and lilac curves show the fit results of the fractions corresponding to D_1, D_2, and D_3, respectively. To see this figure in color, go online.

contribution of the fractions A_i changed over time and depending on the nisin/Lipid II ratio (Fig. 4, *C* and *D*; Fig. S5). Isolated Lipid II-Atto647 molecules represented by A_1 were less frequently observed as the experiment progressed. The effect was more pronounced and occurred faster for the higher nisin concentration. Simultaneously, the contribution of the second fraction A_2 ($D_2 = 2.6$ μm^2/s), representing intermediate aggregate sizes, increased. The third diffusion coefficient $D_3 = 0.3$ μm^2/s was found with a fraction A_3 of 5% only for the high nisin/Lipid II ratio of 30:1 after 20 min incubation. We concluded that the existing intermediate aggregates continued to grow into large aggregates in the presence of 1.5 μM, but not in the presence of 0.2 μM nisin, during the observation period of 20 min.

Equation 3 predicts a logarithmic relationship between the particle radius and diffusion coefficient. However, the model holds only for molecules with a radius smaller than the hydrodynamic length scale $l = (h \cdot \mu_m / \mu_w)$ (31), such as lipids and proteins. Since this was not the case for Lipid II-nisin aggregates, we determined the corresponding particle radii R by means of the analytical expression of Petrov and Schwille (32) given in Eq. 4.

We assumed $R_1 \approx R_{\mathrm{LII}} \approx 0.6$ nm and obtained an averaged radius of $R_2 = 19$ nm for the intermediate aggregates and $R_3 = 1.1$ μm for the large aggregates. Of course, the appropriate approach would be to use a continuous distribution of aggregate radii to fit the data; however, since we had no information about the correct model to describe the size distribution, we preferred this heuristic approach.

We further assumed that aggregates occupied circular areas with radii R_2 and R_3 in the membrane and estimated the number of Lipid II molecules contained within them as the maximum number of circles with radius $R_1 = 0.6$ nm that fit into circular areas with radii R_2 and R_3 (40). This method suggests that ~850 Lipid II molecules were contained in the intermediate aggregates (R_2) and ~1.75×10^6 were contained in the large aggregates (R_3).

These numbers are certainly crude estimates, but they indicate the very large numbers of Lipid II molecules that are required to form aggregates with the observed low mobility.

Nisin-induced aggregation of Lipid II causes membrane budding and GUV destruction

The above-shown mobility studies demonstrated the occurrence of large molecular clusters of membrane-anchored Lipid II with nisin. It is well known that clustering of membrane-bound molecules can lead to distortions of membrane curvature, which can result in membrane rupture and vesicle budding (41,42). In an earlier study, we observed vesicle budding in Lipid II-containing GUVs upon addition of nisin, but only using bright-field microscopy (12). Therefore, vesicle budding could not directly be related to the presence of Lipid II and nisin aggregates at the respective membrane sites. By fluorescently labeling GUVs containing 0.2 mol % Lipid II by POPE-AF546, we created contrast for confocal fluorescence microscopy. In the presence of 0.2 μM nisin-AF647 (nisin/Lipid II ratio 4:1), small aggregates of nisin-AF647 were observed in the membrane, partly colocalizing with small POPE-AF546 lipid clusters (Fig. 5 *A*). In the presence of 1.5 μM nisin-AF647 (nisin/Lipid II ratio 30:1), notably stronger clustering and extensive membrane deformations were observed (Fig. 5 *B*). We observed very bright nisin-AF647 aggregates colocalizing with severe membrane deformations, often resulting in vesicle budding. Interestingly, vesicles formed in both directions, mostly into the exterior but also into the interior of the GUVs (see also Fig. S6).

We presumed that the strong membrane deformations would simultaneously affect GUV stability. Therefore, we monitored the number of GUVs with a radius $R > 10$ μm, N_{GUV}, over time after addition of GUVs to the nisin-containing glucose solution (Fig. 5 *C*). Measurements began
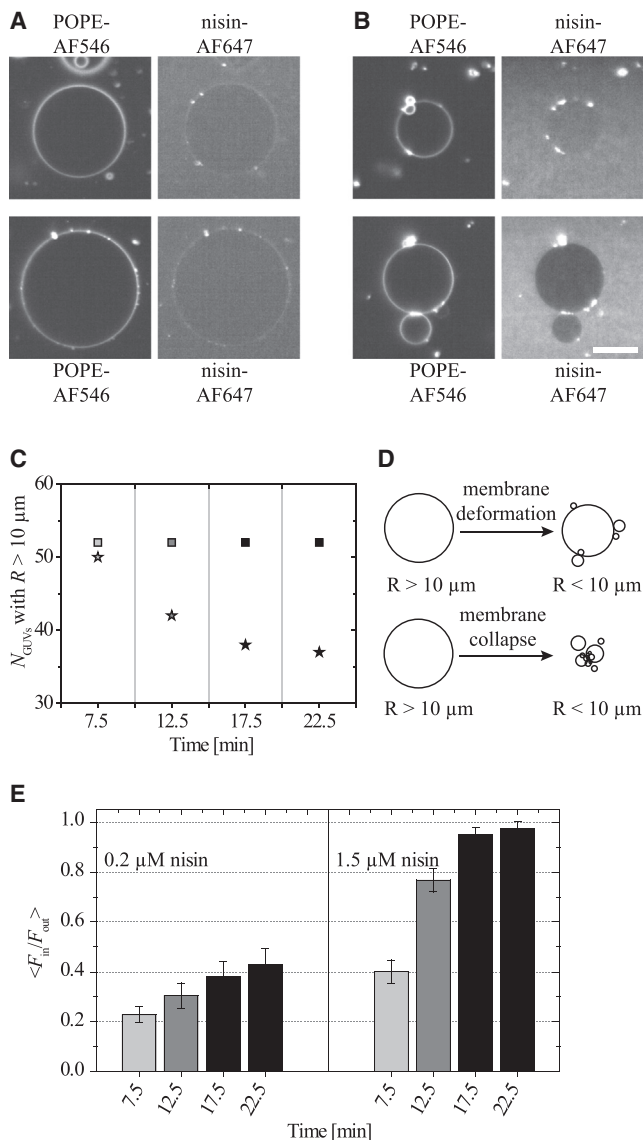
FIGURE 5 GUV destabilization caused by nisin-Lipid II interaction. Vesicle budding of GUVs due to nisin-induced Lipid II aggregation. Example images show the GUVs visualized by a lipid tracer (*left panels*) and nisin-AF647 (*right panels*) bound to Lipid II, which was added at concentrations of (*A*) 0.2 μM and (*B*) 1.5 μM. The higher nisin concentration induced strong membrane deformations and vesicle budding. Scale bar, 20 μm. (*C*) Analysis of the stability of Lipid II-containing GUVs as a function of time after addition of nisin. Initial numbers of vesicles with a diameter $R > 10$ μm were $N_{GUV} = 52$ for 0.2 μM nisin (■, nisin/Lipid II ratio 4:1) and $N_{GUV} = 50$ for 1.5 μM nisin (★, nisin/Lipid II ratio 30:1). (*D*) Schematic representation of GUV radius reduction due to vesicle budding or membrane collapse. (*E*) Membrane perforation was measured by translocation of the tracer LY. The ratio F_{in}/F_{out} of the intensities inside and outside the GUVs was evaluated for 30 GUVs for each nisin concentration. Error bars show the standard error of the mean.

7.5 min after mixing, during which time the GUVs remained stable at the glass chamber bottom. The number of large GUVs ($R > 10$ μm) was constant when 0.2 μM of nisin was added. In contrast to this, approximately one-third of

the initially large GUVs shrank in diameter or collapsed after addition of 1.5 μM nisin and a 25 min incubation. The size reduction was caused either by shape changes due to vesicle budding or by the spontaneous collapse of GUVs (Fig. 5 *D*). Incubation with 1.5 μM nisin caused the collapse of nine out of 50 GUVs.

Membrane permeation efficiency depends on the nisin/Lipid II ratio

Finally, we tested the membrane integrity by using a translocation assay to correlate membrane deformation and a putative leakiness. Membrane perforation was quantitatively analyzed in dependence on the nisin/Lipid II ratio as described previously (12). The translocation of a tracer molecule, the hydrophilic dye LY, was measured by confocal microscopy as a function of time by determining the ratio of its intensity inside the GUVs, F_{in}, and the intensity outside the GUVs, F_{out}. Example time series are shown in Fig. S7. Values of the ratio F_{in}/F_{out} were averaged for 30 GUVs for each nisin concentration (Fig. 5 *E*). An increasing perforation of the GUV membrane over time was observed for both nisin concentrations. Upon addition of 0.2 μM nisin, perforation of Lipid II-containing GUVs was observed, as indicated by a mean fluorescence ratio $<F_{in}/F_{out}> = 0.43$, after a 25 min incubation. The permeation kinetics differed strongly for individual GUVs (12). Not all GUVs were permeated after 25 min. Upon addition of 1.5 μM nisin, however, a mean ratio of $<F_{in}/F_{out}> \approx 1$ was measured after a 25 min incubation, indicating an almost complete equilibration between the GUV interior and exterior for all analyzed GUVs.

These observations show that GUVs were permeated efficiently even at low nisin concentrations, and this did not always lead to visible membrane deformations and never led to vesicle shrinking or destruction of GUVs. Obviously, membrane perforation could occur before notable vesicle budding. However, membranes were very efficiently perforated when more nisin and thus larger aggregates were present and visible membrane perturbations occurred.

DISCUSSION

The lantibiotic nisin is an AMP whose antimicrobial capacity relies on specific binding to bacterial Lipid II. Hasper et al. (11) imaged fluorescently labeled nisin on fixed cells and observed the formation of large nisin aggregates on the bacterial cell membranes. However, these authors could not clearly reveal the biological impact of the formation of large aggregates. In a recent study (12) we showed that in these nisin aggregates, large numbers of Lipid II molecules always colocalize. Here, we analyzed the biological relevance of aggregate formation between nisin and Lipid II in membranes of *B. subtilis* and in vitro.

Biological relevance of nisin-Lipid II aggregates

Fluorescence microscopic imaging revealed that nisin aggregation occurred within 20 min after binding to bacterial cells and resulted in high local concentrations of fluorescent nisin. Using a membrane-impermeant fluorescent marker, we correlated membrane integrity and cell viability with nisin aggregation. Membrane damage and cell death were found only above a certain nisin aggregate intensity. This suggested that membrane damage and cell death appeared after nisin aggregates reached a certain size, and demonstrated the biological importance of large-scale aggregation for the killing mechanism of nisin.

The number of Lipid II molecules in Gram-positive bacteria is estimated to be 35,000–200,000 molecules per cell (43). In the exponential growth phase, Lipid II is located at the septum of *B. subtilis* (44), where it is produced by the protein complexes of the cell wall biosynthesis machinery. Accordingly, large nisin aggregates were found at regions of Lipid II synthesis and activity, namely, in the middle and the poles of the cells where cell division and cell elongation take place, respectively. It was not straightforward to determine the number of fluorescent nisin molecules in the aggregates in the bacterial membranes. Therefore, we turned to study the nisin-induced aggregation process in GUV membranes that contained fluorescently labeled Lipid II molecules, and analyzed the effect of nisin on Lipid II mobility and GUV integrity by high-speed fluorescence microscopy.

Size of nisin-Lipid II aggregates

The relation between diffusion coefficient and particle size (32) allowed us to determine the effective radii of nisin-Lipid II aggregates in GUV membranes containing POPC. We assessed the number of molecules contained in the aggregates by using a simple geometric approximation. We found that ~800 and up to 10^6 Lipid II molecules were contained in intermediate and large aggregates with effective radii of 19 nm and 1 μm, respectively. In the estimate, we neglected the area contribution of nisin as well as phospholipid molecules, which most probably were also contained in the aggregates. Nevertheless, the dimension of the given numbers revealed that the Lipid II content in the aggregates is several orders of magnitude higher than predicted for nisin-Lipid II oligomers in a previous pore model (13).

Aggregation of nisin and Lipid II

To elucidate the kinetics of the aggregation process of nisin-Lipid II complexes, we measured the diffusion of Lipid II particles and attributed the changes in mobility states to a growth of nisin-Lipid II aggregates. We found that Lipid II mobility in GUV membranes steadily decreased over 20 min in the presence of nisin. The effect was more pronounced at a higher nisin/Lipid II ratio.

In our measurements, we observed no specific intermolecular interactions between Lipid II molecules alone in the POPC bilayers. One nisin probably binds only a single Lipid II molecule (6), and a direct cross-linking between several molecules is hard to imagine. Rather, we observed a situation comparable to an ideal two-dimensional solution with Lipid II as solute and POPC as solvent. The binding of nisin to the pyrophosphate group of Lipid II induced its aggregation, converting an ideal solution to a real solution in which interactions between the solute molecules exist. If in such solutions the interaction energy of the solute is large enough to overcome the translational entropy, segregation of the solute will take place. Membrane-mediated forces alone may be responsible for such a segregation. These could be generated by conformational changes of nisin (7) upon binding to Lipid II, leading to deeper insertion of Lipid II into the membrane (8,37). Insertion of amphipathic peptides into lipid bilayers enhances the interfacial energy of the bilayer, which can lead to phase separation into peptide-enriched and peptide-depleted phases according to theoretical calculations of Zemel et al. (45), to again minimize free energy. Accordingly, experiments using the distance-dependent self-quenching of fluorescently labeled peptides proved the clustering and arrangement of peptides in ordered mesophases with increasing membrane concentration (46). Furthermore, simulations indicated that curvature induction could also be a driving force for peptide aggregation. Reynwar et al. (47) showed that after a minimal local bending was reached, the clustering of model proteins was induced without specific interactions.

Effect of aggregation on membrane shape

Upon addition of nisin to the Lipid II-containing GUVs, we observed the formation of vesicle buds. This indicated that bilayer organization was heavily affected by the progressive aggregate growth. Induction of membrane curvature due to asymmetric adsorption of particles is well known and depends on the size of the absorbed particles (48). Theoretically, it was predicted that after a critical aggregate size is reached, vesicle buds form as a consequence of bending energy minimization (49). Indeed, we noted that formation of large nisin-Lipid II aggregates at GUV membranes was required to provoke vesicle budding. Membrane shape transformations, such as vesicle budding, often destroy the barrier function of membranes.

Aggregate size and membrane permeation capacity

Membrane permeability was assessed by confocal imaging of the fluorescent tracer LY outside and inside of single GUVs. These experiments revealed that increasing the nisin/Lipid II ratio from 4:1 to 30:1 not only led to the formation of larger aggregates but also increased membrane

permeation. For the lower nisin concentrations, ~50% equilibration was reached on average after 25 min, whereas for the high nisin concentration, virtually all GUVs were perforated and completely equilibrated.

In contrast to this, previous fluorescence spectroscopic measurements on DOPC large unilamellar vesicles (LUVs) doped with pyrene-labeled Lipid II showed that saturation of excimer formation was reached at a nisin/Lipid II ratio of 2:1 (13), and membrane permeation activity was not further increased with higher nisin/Lipid II ratios (6). We suspect that membrane permeation depends not only on the nisin/Lipid II ratio but also on the intrinsic membrane curvature, which is much higher in LUVs than in GUVs. Hence, the formation of small aggregates might be sufficient to cause membrane deformations in smaller vesicles.

In addition, earlier black lipid membrane studies indicated the formation of stable nisin-Lipid II pores with an average channel diameter of 2–2.5 nm (9). The existing model describes the channel structure as a classical pore consisting of four Lipid II and eight nisin molecules with a transmembrane orientation (8,13). These results suggest that indeed very small oligomeric Lipid II-nisin aggregates would lead to the membrane permeation effects that occurred in our experiments. However, a back-of-the-envelope calculation rules out the possibility that small pores containing only a few Lipid II molecules could cause the observed membrane permeability for LY. An average GUV with a diameter of 20 μm comprised ~2×10^9 phospholipids and 4×10^6 Lipid II molecules. It was found that 2×10^6 Lipid II molecules were located on the GUV outside, and 80% of these formed a 1:1 complex in the presence of 0.2 μM nisin, assuming a binding constant $K_b = 2 \times 10^7 \text{ M}^{-1}$ (6). This yields a total number of 1.6×10^6 Lipid II-nisin complexes in the outer GUV monolayer. Estimation of the transport capacity of a single pore (inner $\varnothing$, 2 nm) for the tracer LY (molecular $\varnothing$, 1 nm) yields a time span of 20–25 min until equilibration due to diffusive transport between the GUV exterior and interior (50–52). The presence of 100 pores would reduce this time to only 15 s. Thus, if the transport were to occur via such small (but presumably frequent) pores, equilibration would take place within seconds, and not within 25 min. Hence, our translocation data clearly argue against a role of small oligomeric channels.

CONCLUSIONS

In summary, we conclude that three experimental results argue for a biological relevance of large Lipid II-nisin aggregates: 1) the strong correlation among large nisin aggregates, bacterial cell death, and membrane disruption; 2) the rapid growth of nisin-Lipid II aggregates comprising hundreds of molecules in vitro; and 3) the slow permeation of GUVs for tracer molecules in the presence of high numbers of Lipid II-nisin complexes.

SUPPORTING MATERIAL

Seven figures, one table, and one movie are available at http://www.biophysj.org/biophysj/supplemental/S0006-3495(15)00114-9.

REFERENCES

1. Brogden, K. A. 2005. Antimicrobial peptides: pore formers or metabolic inhibitors in bacteria? *Nat. Rev. Microbiol.* 3:238–250.

2. Shai, Y. 1999. Mechanism of the binding, insertion and destabilization of phospholipid bilayer membranes by alpha-helical antimicrobial and cell non-selective membrane-lytic peptides. *Biochim. Biophys. Acta.* 1462:55–70.

3. Boheim, G. 1974. Statistical analysis of alamethicin channels in black lipid membranes. *J. Membr. Biol.* 19:277–303.

4. Ludtke, S. J., K. He, …, H. W. Huang. 1996. Membrane pores induced by magainin. *Biochemistry.* 35:13723–13728.

5. Parton, D. L., E. V. Akhmatskaya, and M. S. P. Sansom. 2012. Multi-scale simulations of the antimicrobial peptide maculatin 1.1: water permeation through disordered aggregates. *J. Phys. Chem. B.* 116: 8485–8493.

6. Wiedemann, I., E. Breukink, …, H. G. Sahl. 2001. Specific binding of nisin to the peptidoglycan precursor Lipid II combines pore formation and inhibition of cell wall biosynthesis for potent antibiotic activity. *J. Biol. Chem.* 276:1772–1779.

7. Hsu, S. T. D., E. Breukink, …, N. A. J. van Nuland. 2004. The nisin-Lipid II complex reveals a pyrophosphate cage that provides a blueprint for novel antibiotics. *Nat. Struct. Mol. Biol.* 11:963–967.

8. van Heusden, H. E., B. de Kruijff, and E. Breukink. 2002. Lipid II induces a transmembrane orientation of the pore-forming peptide lantibiotic nisin. *Biochemistry.* 41:12171–12178.

9. Wiedemann, I., R. Benz, and H. G. Sahl. 2004. Lipid II-mediated pore formation by the peptide antibiotic nisin: a black lipid membrane study. *J. Bacteriol.* 186:3259–3261.

10. Breukink, E., H. E. van Heusden, …, B. de Kruijff. 2003. Lipid II is an intrinsic component of the pore induced by nisin in bacterial membranes. *J. Biol. Chem.* 278:19898–19903.

11. Hasper, H. E., N. E. Kramer, …, E. Breukink. 2006. An alternative bactericidal mechanism of action for lantibiotic peptides that target Lipid II. *Science.* 313:1636–1637.

12. Scherer, K., I. Wiedemann, …, U. Kubitscheck. 2013. Aggregates of nisin with various bactoprenol-containing cell wall precursors differ in size and membrane permeation capacity. *Biochim. Biophys. Acta.* 1828:2628–2636.

13. Hasper, H. E., B. de Kruijff, and E. Breukink. 2004. Assembly and stability of nisin-Lipid II pores. *Biochemistry.* 43:11567–11575.

14. Spille, J. H., T. Kaminski, …, U. Kubitscheck. 2012. Dynamic three-dimensional tracking of single fluorescent nanoparticles deep inside living tissue. *Opt. Express.* 20:19697–19707.

15. Gross, E., and J. L. Morell. 1971. The structure of nisin. *J. Am. Chem. Soc.* 93:4634–4635.

16. Mulders, J. W., I. J. Boerrigter, …, W. M. de Vos. 1991. Identification and characterization of the lantibiotic nisin Z, a natural nisin variant. *Eur. J. Biochem.* 201:581–584.

17. Zendo, T., M. Fukao, …, K. Sonomoto. 2003. Identification of the lantibiotic nisin Q, a new natural nisin variant produced by Lactococcus

lactis 61-14 isolated from a river in Japan. *Biosci. Biotechnol. Biochem.* 67:1616–1619.

18. Wirawan, R. E., N. A. Klesse, …, J. R. Tagg. 2006. Molecular and genetic characterization of a novel nisin variant produced by Streptococcus uberis. *Appl. Environ. Microbiol.* 72:1148–1156.

19. Kuipers, O. P., H. S. Rollema, …, W. M. de Vos. 1992. Engineering dehydrated amino acid residues in the antimicrobial peptide nisin. *J. Biol. Chem.* 267:24340–24346.

20. Bonelli, R. R., T. Schneider, …, I. Wiedemann. 2006. Insights into in vivo activities of lantibiotics from gallidermin and epidermin mode-of-action studies. *Antimicrob. Agents Chemother.* 50:1449–1457.

21. Schneider, T., M. M. Senn, …, I. Wiedemann. 2004. In vitro assembly of a complete, pentaglycine interpeptide bridge containing cell wall precursor (Lipid II-Gly5) of Staphylococcus aureus. *Mol. Microbiol.* 53:675–685.

22. Moumtzi, A., M. Trenker, …, A. Hermetter. 2007. Import and fate of fluorescent analogs of oxidized phospholipids in vascular smooth muscle cells. *J. Lipid Res.* 48:565–582.

23. Dimitrov, D. S., and M. I. Angelova. 1988. Lipid swelling and liposome formation mediated by electric fields. *J. Electroanal. Chem. Interfacial Electrochem.* 253:323–336.

24. Menger, F. M., and J. S. Keiper. 1998. Chemistry and physics of giant vesicles as biomembrane models. *Curr. Opin. Chem. Biol.* 2:726–732.

25. Ciobanasu, C., E. Harms, …, U. Kubitscheck. 2009. Cell-penetrating HIV1 TAT peptides float on model lipid bilayers. *Biochemistry.* 48:4728–4737.

26. Ritter, J. G., R. Veith, …, U. Kubitscheck. 2010. Light sheet microscopy for single molecule tracking in living tissue. *PLoS ONE.* 5:e11639.

27. Schneider, C. A., W. S. Rasband, and K. W. Eliceiri. 2012. NIH Image to ImageJ: 25 years of image analysis. *Nat. Methods.* 9:671–675.

28. Anderson, C. M., and G. N. Georgiou, …, R. J. Cherry. 1992. Tracking of cell surface receptors by fluorescence digital imaging microscopy using a charge-coupled device camera. Low-density lipoprotein and influenza virus receptor mobility at 4 degrees C. *J. Cell Sci.* 101:415–425.

29. Schütz, G. J., H. Schindler, and T. Schmidt. 1997. Single-molecule microscopy on model membranes reveals anomalous diffusion. *Biophys. J.* 73:1073–1080.

30. Saffman, P. G., and M. Delbrück. 1975. Brownian motion in biological membranes. *Proc. Natl. Acad. Sci. USA.* 72:3111–3113.

31. Hughes, B. D., B. A. Pailthorpe, and L. R. White. 1981. The translational and rotational drag on a cylinder moving in a membrane. *J. Fluid Mech.* 110:349–372.

32. Petrov, E. P., and P. Schwille. 2008. Translational diffusion in lipid membranes beyond the Saffman-Delbruck approximation. *Biophys. J.* 94:L41–L43.

33. Roth, B. L., M. Poot, …, P. J. Millard. 1997. Bacterial viability and antibiotic susceptibility testing with SYTOX green nucleic acid stain. *Appl. Environ. Microbiol.* 63:2421–2431.

34. Kučerka, N., M. P. Nieh, and J. Katsaras. 2011. Fluid phase lipid areas and bilayer thicknesses of commonly used phosphatidylcholines as a function of temperature. *Biochim. Biophys. Acta.* 1808:2761–2771.

35. Lide, D. R. 2012. CRC Handbook of Chemistry and Physics, 92nd ed. CRC Press Taylor & Francis Group, Boca Raton.

36. Kramer, N. E., E. J. Smid, …, E. Breukink. 2004. Resistance of Gram-positive bacteria to nisin is not determined by Lipid II levels. *FEMS Microbiol. Lett.* 239:157–161.

37. Koch, D. C., T. H. Schmidt, …, C. Kandt. 2014. Structural dynamics of the cell wall precursor Lipid II in the presence and absence of the lantibiotic nisin. *Biochim. Biophys. Acta.* 1838:3061–3068.

38. de Vos, W. M., J. W. M. Mulders, …, O. P. Kuipers. 1993. Properties of nisin Z and distribution of its gene, nisZ, in Lactococcus lactis. *Appl. Environ. Microbiol.* 59:213–218.

39. Speil, J., and U. Kubitscheck. 2010. Single ovalbumin molecules exploring nucleoplasm and nucleoli of living cell nuclei. *Biochim. Biophys. Acta.* 1803:396–404.

40. Specht, E. 2014. The best known packings of equal circles in a circle (complete up to N = 2600). August 6, 2014. http://hydra.nat.uni-magdeburg.de/packing/cci/.

41. Tribet, C., and F. Vial. 2008. Flexible macromolecules attached to lipid bilayers: impact on fluidity, curvature, permeability and stability of the membranes. *Soft Matter.* 4:68–81.

42. Schmidt, N. W., A. Mishra, …, G. C. L. Wong. 2011. Criterion for amino acid composition of defensins and antimicrobial peptides based on geometry of membrane destabilization. *J. Am. Chem. Soc.* 133:6720–6727.

43. van Heijenoort, J. 2007. Lipid intermediates in the biosynthesis of bacterial peptidoglycan. *Microbiol. Mol. Biol. Rev.* 71:620–635.

44. Daniel, R. A., and J. Errington. 2003. Control of cell morphogenesis in bacteria: two distinct ways to make a rod-shaped cell. *Cell.* 113:767–776.

45. Zemel, A., A. Ben-Shaul, and S. May. 2004. Membrane perturbation induced by interfacially adsorbed peptides. *Biophys. J.* 86:3607–3619.

46. Aisenbrey, C., and B. Bechinger. 2014. Molecular packing of amphipathic peptides on the surface of lipid membranes. *Langmuir.* 30:10374–10383.

47. Reynwar, B. J., G. Illya, …, M. Deserno. 2007. Aggregation and vesiculation of membrane proteins by curvature-mediated interactions. *Nature.* 447:461–464.

48. Lipowsky, R. 2013. Spontaneous tubulation of membranes and vesicles reveals membrane tension generated by spontaneous curvature. *Faraday Discuss.* 161:305–331, discussion 419–459.

49. Tsai, F. C., and H. Y. Chen. 2008. Adsorption-induced vesicle fission. *Phys. Rev. E Stat. Nonlin. Soft Matter Phys.* 78:051906.

50. Tschödrich-Rotter, M., U. Kubitscheck, …, R. Peters. 1996. Optical single-channel analysis of the aerolysin pore in erythrocyte membranes. *Biophys. J.* 70:723–732.

51. Noskov, S. Y., W. Im, and B. Roux. 2004. Ion permeation through the alpha-hemolysin channel: theoretical studies based on Brownian dynamics and Poisson-Nernst-Plank electrodiffusion theory. *Biophys. J.* 87:2299–2309.

52. Schwarz, G., and C. H. Robert. 1992. Kinetics of pore-mediated release of marker molecules from liposomes or cells. *Biophys. Chem.* 42:291–296.